High-temperature oxidation kinetics of NiAl single crystal and oxide spallation as a function of crystallographic orientation

Dominique Poquillon, Djar Oquab, Bernard Viguier, François Senocq, Daniel Monceau

High-temperature oxidation kinetics of NiAl single crystal and oxide spallation as a function of crystallographic orientation

D. Poquillon*, D. Oquab, B. Viguier, F. Sénocq, D. Monceau

CIRIMAT, INPT/ENSIACET, 118 Route de Narbonne, F-31077 Toulouse Cedex 04, France

Abstract

Isothermal and cyclic high-temperature oxidation of NiAl single crystal samples are presented. Oxidations have been carried out at 900, 1050, 1100 and 1150 °C on (1 0 0) and (1 1 0) oriented surface. Continuous thermogravimetry in cyclic conditions allows isothermal oxidation kinetics and spalling at each cycle to be followed. Oxidation kinetics are compared between (1 0 0) surface and (1 1 0) surface. (1 0 0) oriented surfaces appeared to oxidize slightly faster than (1 1 0) oriented surfaces. Experimental results of cyclic oxidation are compared to simulated results using a previously published statistical model. Spalling increases when the average oxide scale thickness increases with the number of cycles. Longer tests are necessary to study this evolution during the 'steady-state' but no critical oxide thickness was found.

Keywords: Cyclic oxidation kinetics; NiAl; Spalling; Alumina formers; Cyclic thermogravimetry

1. Introduction

To improve gas turbine engine performance, Ni-based superalloys are overlaid with an oxidation resistant metallic coating. During high-temperature operation, the coating oxidizes to form an alumina protective oxide scale. Life duration of such a system depends on the adherence of this scale and on the ability of the material to redevelop this protective alumina scale when spalling occurs. Gas turbine engine components are submitted to cyclic thermo-mechanical loading. The thermal expansion mismatch between metal and oxide induces stresses during heating and cooling. These stresses may lead to dramatic degradation. Many studies had been devoted to this subject. In the present work we have chosen to study single crystal β-NiAl because this phase is a major component of diffusion coatings used on Ni-based superalloys. Furthermore, β-NiAl oxidation produces only alumina and oxidation mechanisms are easier to understand [1].

Both Smialek et al. [2,3] have used kinetics models to fit NiAl cyclic oxidation. In a former study [4], we applied the analytical solution of a simple model similar to the one proposed by Smialek [2] to analyze cyclic oxidation results and to give a first estimate of lifetime concerning nickel aluminide oxidation. This model appeared to fit quite well data available in the literature. In the present work, we performed specific oxidation tests in order to measure oxidation kinetics and alumina spalling on single crystal NiAl for two different crystallographic orientations. Furthermore, experimental results during isothermal oxidation tests allow us to compare oxidation kinetics and spalling between the (1 0 0) and the (1 1 0) oriented surfaces. Then, we applied the proposed model to the experimental data. At the end, the model is discussed and criticized.

2. Experimental procedures

The NiAl single crystal was provided by ONERA. Its chemical composition is given in Table 1. The single crystal rod was grown approximately along ⟨0 0 1⟩ direction. More precise (within about 1 *deg*) orientation of the specimen were obtained using back Laue diffraction technique. The rod was successively oriented along the [0 0 1], then the [1 1 0] direction. In both cases, 1 mm thick slices were electro-discharge machined. The samples were egg-shaped disks, with a 10 mm nominal diameter. A part of the rod was flattened and the crystallographic direction of this segment

* Corresponding author. Tel.: +33-562885662; fax: +33-562885663.
E-mail address: Dominique.Poquillon@ensiacet.fr (D. Poquillon).

doi:10.1016/j.msea.2004.04.009

Table 1
NiAl single crystal composition

Ni	Al (at.%)	Fe (at. ppm)	S (at. ppm)	Mg (at. ppm)	Si (at. ppm)
Balance	45.6	111	42	120	525

roughly determined so that it was possible to orientate any direction on the specimen surface.

For each sample, the surfaces were carefully polished (0.25 μm) and cleaned (ultrasonic bath of alcohol, acetone, methanol). Except for the test labelled A12, high-temperature oxidation tests were conducted in a SETARAM TAG24S equipment at 900, 1050, 1100 and 1150 °C. In this device, sample and countersample are both hanged in their furnace with the same Pt hang wire. They are submitted to the same gas flow and heated at the same temperature. So, Pt evaporation from the wire, which could occur in such an experiment is supposed to be equal on both side. As only the mass difference is measured between the sample and the inert countersample, Pt evaporation of the hang wire should not interfere with kinetics measurements.

Except for the shortest tests (A10, A15), all the tests were carried out entirely in 1 atm flowing oxygen. Low oxygen partial pressures combined with a grit blasted surface promote α-alumina instead of θ-alumina during the heating of sample under argon [5]. For this study, it was not possible to apply grit blasting to the surface of the sample, nevertheless, heating under argon was tested on the samples A10 and A15 to try to increase the α-alumina/θ-alumina ratio.

Test characteristics are given in Tables 2 and 3. For isothermal tests, heating and cooling were performed at $1\,^{\circ}s^{-1}$. The same heating and cooling rate was used for cyclic tests as this parameter is important for transient oxidation [5]. The low-temperature hold of the cycle was fixed at 150 °C. Test A3 was realized in three sequences introducing two long dwell times at room temperature in the same atmosphere without taking out the sample. These two sequences led to quite different results from those obtained when cooling the sample down to 150 °C. This point will be discussed later. Test A12 was carried out in an horizontal cyclic oxidation device in laboratory air. Cooling and heating rates were 20 K/s. Samples were weighted after 2, 4, 10, 14 cycles and then every 18 cycles.

The alumina scale formed during oxidation was analyzed with XRD. The data were collected with a Seifert XRD 3000 TT diffractometer in grazing 5° incidence configuration, using Cu Kα radiation, and fitted with a diffracted-beam graphite monochromator. The data were collected in a [10–45°]Θ Bragg range. For samples A16 and A18 several incidence angles were used (0.5 and 1–20° by 1° steps).

The samples were observed with a scanning electron microscope (LEO 435VP). Most of the observations were performed in secondary electron imaging under 15 kV voltage with a current of 80 pA in the specimen. This procedure allowed us to observe raw specimens without metallising.

Table 2
Isothermal oxidation tests (flowing O_2 during dwell)

Sample	Surface orientation	Temperature (°C)	Oxidation duration (s)	k_p ($mg^2\,cm^{-4}\,s^{-1}$)
A4	(1 0 0)	1150	64800	8.0×10^{-7}
A11	(1 0 0)	1100	60	7.9×10^{-7}
A16	(1 0 0)	1050	3605	8.4×10^{-7}
A1	(1 0 0)	900	17187	4.7×10^{-7}
A6	(1 0 0)	900	18843	3.3×10^{-7}
A13	(1 0 0)	900	3688	4.1×10^{-7}
A14	(1 0 0)	900	21615	1.7×10^{-7}
A7	(1 1 0)	1150	72000	7.3×10^{-7}
A10	(1 1 0)	1150	360	2.2×10^{-6}
A15	(1 1 0)	1150	60	1.8×10^{-5}
A18	(1 1 0)	1050	2783	7.0×10^{-7}

2.1. The parabolic constant k_p evaluation

Even for isothermal oxidation experiments, the determination of the parabolic constant k_p requires a careful analysis [6] and most of the experimental data do not follow simple parabolic kinetics, but include a transient oxidation stage (generally with higher oxidation kinetics) before a period of 'pseudo-steady' state oxidation with parabolic kinetics. In this study, k_p was evaluated when the 'pseudo-steady' state was reached as detailed in [6]. Concerning cyclic oxidation, a parabolic mass gain could be observed during the high-temperature hold times. But, as explained elsewhere [7], the k_p calculated at each dwell time slightly overestimates local oxidation kinetics because of the non-uniform thickness of the oxide scale.

2.2. Spalling evaluation

During cyclic testing, the use of continuous thermogravimetry in cyclic conditions allows a quantitative evaluation of spalling [7]. Mass can only be compared at equal

Table 3
Cyclic oxidation test characteristics (carried out under flowing O_2 except A12 in laboratory air)

Sample	Surface orientation	Temperature (°C)	Dwell duration (h)	Number of cycles	Comment
A3	(1 0 0)	1150	1	150	3 × 50 cycles
A5	(1 0 0)	1150	0.75	170	
A8	(1 1 0)	1150	0.75	60	
A12	(1 1 0)	1050	0.75	970	Air, cyclic device
A17	(1 1 0)	1150	0.75	20	incident

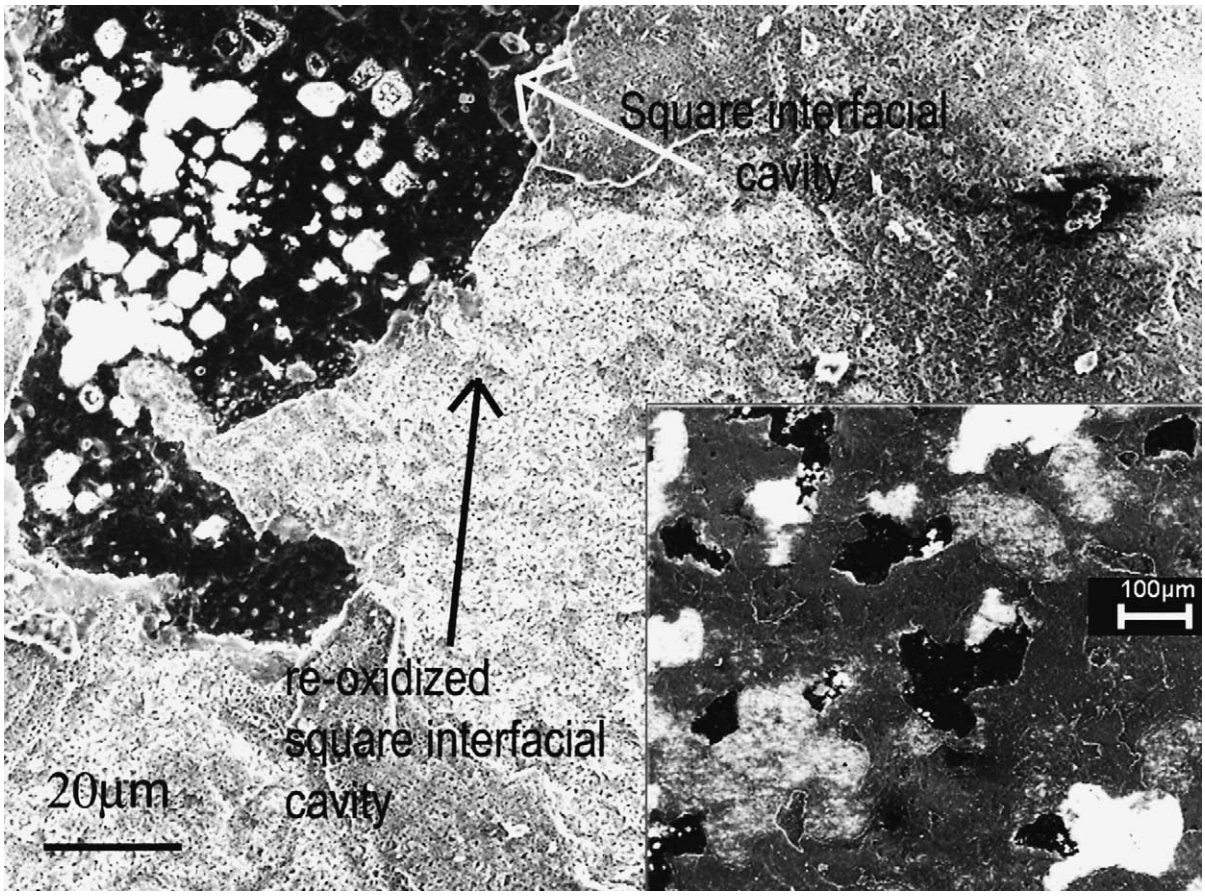

Fig. 1. Cyclic oxidation (Test A3: 150 1 h cycles at 1150 °C). S.E.M. observation of the (1 0 0) surface. Bare metal (spalling occurs at metal–oxide interface), alumina, re-oxidized zones and square interfacial cavities are evidenced. Right corner picture shows the macroscopic aspect of the spalling and of the re-oxidizing.

temperature because of convection and of buoyancy effects. To quantify spalling during these experiments, we performed a careful analysis of the mass gain signal. S.E.M. examinations showed that oxide scale spalled partly during the cooling. Some spalled areas were re-oxidized while others are not oxidized (Fig. 1). This observation proved that spalling occurred during the cyclic experiments and not only when cooling the sample to room temperature. For all the tests performed in this study, oxide scale spalling always occurred at the metal/oxide interface, leaving a bare alloy surface which will locally oxidize at a high rate during the next high-temperature dwell. This high rate is due to parabolic oxidation kinetics for which the rate of oxidation is maximum at the initial stage, and due to transient alumina formation (θ-alumina has higher growth kinetics than α-alumina).

For quantitative evaluation of spalling, we decided to neglect oxidation during heating and cooling. Then we defined the experimental spalling S^n_{OX} at cycle number n as the difference between the mass M^n_{end} of the sample at the end of cycle n (just before cooling) and the mass M^{n+1}_{bg} of the sample at the beginning of the $n+1$ dwell time. We defined oxide growth during cycle n : O^n_x (oxygen pick up to form the oxide) as the difference between the mass of the sample at the end M^n_{end} and at the beginning M^n_{bg} of a dwell time. So we have:

$$S^n_{OX} = M^{n+1}_{bg} - M^n_{end} \quad \text{and} \quad O^n_x = M^n_{end} - M^n_{bg} \tag{1}$$

The main error of such an analysis is that spalling is underestimated because of oxide growth during heating and cooling. This point is particularly evident during the first cycles where this method can give positive value for S^n_{OX} [7].

The total substrate mass modification Met^n (metal consumption) at cycle n (in fact always negative) is directly related to O^n_x. The oxygen is picked up from the flowing gas to form the oxide, whereas metal comes from the substrate. So, the metal consumption is linked to the mass of oxygen picked up through the stoichiometric ratio $(2\times27)/(3\times16)$.

$$Met^n = Met^{n-1} - \frac{54}{48}O^n_x; \tag{2}$$

The adherent oxide mass at the end cycle n, A^n_{OX}, is:

$$A^n_{OX} = A^{n-1}_{OX} + \frac{102}{48}O^n_x + S^n_{OX} \tag{3}$$

The proportion of the mass of the adherent oxide which spalled at cycle n is defined as the following ratio:

$$P_n = \frac{-S^n_{OX}}{A^n_{OX}} \quad (4)$$

Using this method, we can describe the history of the sample:

- Net mass gain: $NMG^n = M^{n+1}_{bg}$
- Substrate mass loss: Met^n
- Adherent oxide mass: A^n_{OX}
- Cumulated total mass gain (gross mass gain): $GMG_n = \sum_{j=1}^{n}(M^j_{end} - M^j_{bg})$

Cyclic tests are listed in Table 3. For the three cyclic tests performed in the Setaram TAG24S (A3, A5 and A8), we were able to assess spalling and oxidation rate for each cycle. For the test labelled A17, the symmetric furnace with the counterweight sample broke down during the first cycle and the TAG data signal was useless. However, S.E.M. observations and XRD analysis were carried out on that sample. The oxide thickness measured was in agreement with data obtained during test A8. Test A12 was performed under different conditions, on a cyclic oxidation experimental device in which sample was not continuously weighed. So, only the net mass gain curve was obtained but for a longer oxidation duration (970 1 h-cycles). The simple cyclic oxidation model p–k_p can also be used for this test.

3. Results and discussion

We will first described isothermal test results, then cyclic test results. The effect of surface orientation on oxidation kinetics and on spalling will be detailed. In the last part, we will focuss on cyclic oxidation and compare experimental data obtained to the previously proposed model.

3.1. Isothermal test results

Isothermal oxidation performed at different temperatures led to different final oxide structures and thicknesses. Mass gain curves during the high-temperature hold are given in Fig. 2. Oxidation kinetics appear to be parabolic and slowly decreased after 1 h for the longest tests. The shortest tests (A10, A15) performed at the highest temperature (1150 °C) produced mainly θ-alumina with some α-alumina, even when the heating was performed under argon. Tests carried out at 900 °C produced only θ-alumina. The other tests produced mainly α-alumina with a porous cellular external layer and a compact inner layer (Fig. 3). It was not possible to produce an α-alumina layer thinner than 1 μm on a polished (mirror finish) NiAl surface in this study. A previous study [5] showed that a grit blasted finish was necessary to produce a thin α-alumina layer at 900–1000 °C on (Ni, Pd)Al. No obvious difference could be detected between samples A16 and A18 which were oxidized under the same conditions, also they differed by their surface crystallographic orientation.

On the two samples, the varying incidence XRD analysis showed that the transition alumina layer was located on the top of the α-alumina layer (Fig. 4). Net mass gain curves obtained during the 10 isothermal tests allowed the calculation of different k_p values which are given in Table 2. They are also plotted in an Arrhenius diagram in Fig. 5.

It is well known [8], under conditions of this study, that θ-alumina grows faster than α-alumina. Then θ-alumina, which is metastable, transforms into α-alumina. The kinetics of this transformation are temperature-dependent. According to [9], when Fe20Cr-5Al is oxidized at 1050 °C, no more θ-alumina is detected after 1 h. Data obtained here on NiAl

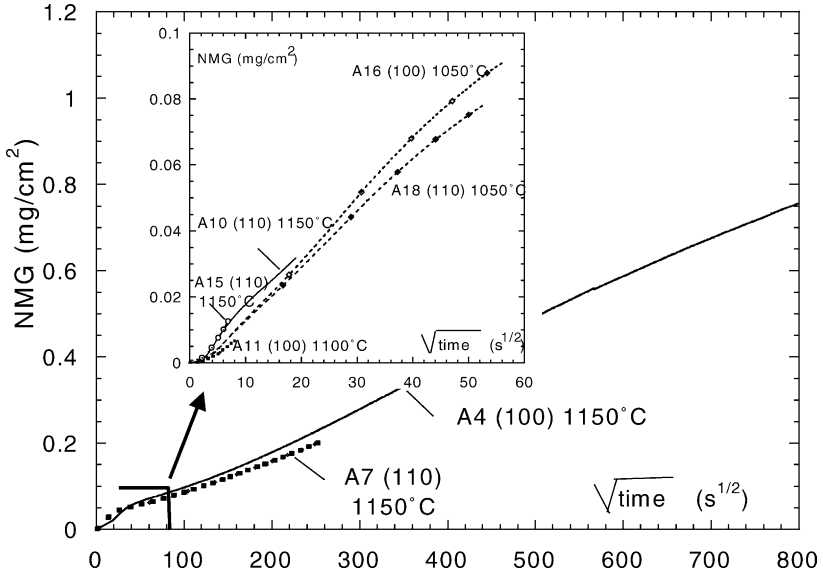

Fig. 2. Mass gain curve obtained during isothermal oxidation tests under flowing O_2 plotted versus square root of time. Net mass gain is roughly parabolic. Orientation effect is evidenced at 1050 °C between tests A16 and A18 and at 1150 °C between tests A4 and A7.

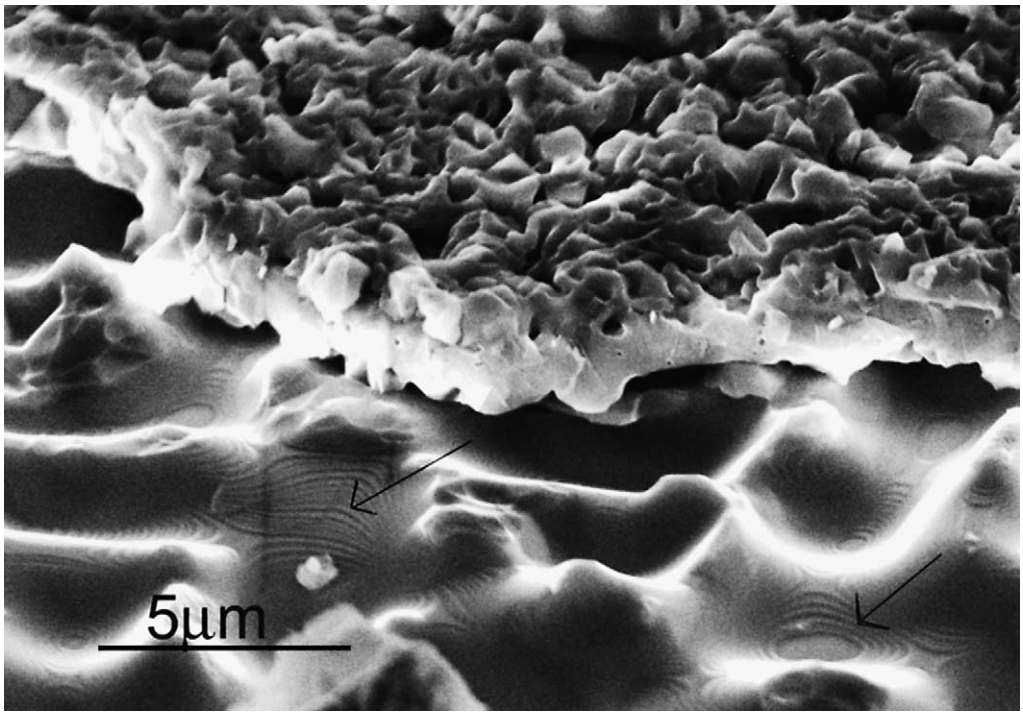

Fig. 3. Isothermal oxidation (Test A7, 20 h at 1150 °C, in flowing O_2). S.E.M.–S.E. observation of the (1 1 0) surface. Arrows indicate steps on β-NiAl surface.

are consistent with this result on FeCrAl. The k_p values measured in the present study lie between the literature data for α-alumina and θ-alumina. For the two longest isothermal tests (A4 and A7) after about 1 h at 1150 °C, the slope of the net mass gain curves plotted versus the square root of time decreases and then remains constant. The values reported in Table 2 are calculated during the second stage which corresponds to the formation of α-alumina. The k_p values calculated for the first hour of oxidation of tests A4 (64800 s at 1150 °C) and A7 (72000 s at 1150 °C) are in the same range as the values obtained at the same temperature for test A10 (360 s at 1150 °C) and A15 (60 s at 1150 °C). Test A15 (60 s) was very short and the oxide mass formed during the time at high temperature was comparable to that formed during heating. XRD analysis detected only θ-alumina on this last sample.

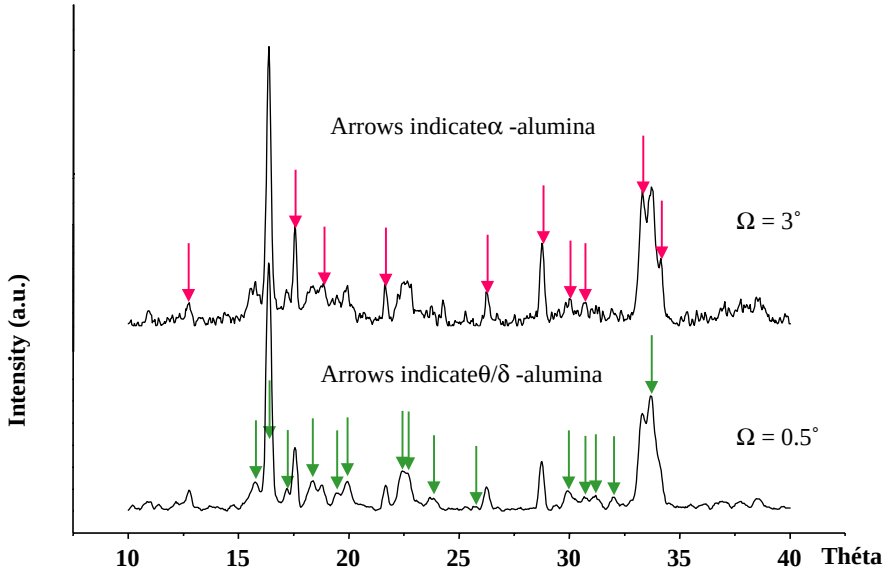

Fig. 4. Grazing incidence X-rays diffraction of NiAl sample A18 oxidized at 1050 °C during 2783 s in flowing O_2, showing more α-alumina at a 3° incidence and more transition alumina at 0.5°.

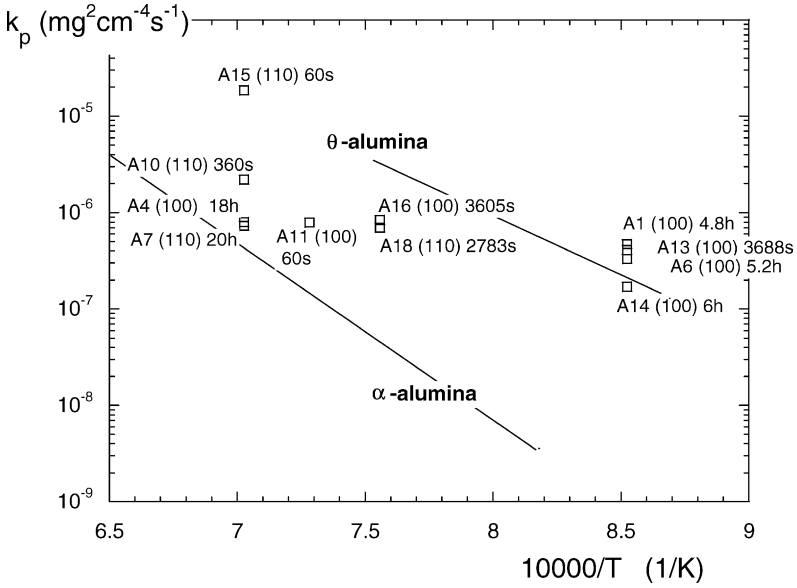

Fig. 5. Arrhenius plot of the parabolic rate constant k_p (data lines for α-alumina and θ-alumina are from [8]).

3.2. Cyclic test results

These tests (A3, A5, A8, A12, A17) produced mainly α-alumina. No significant difference between the isothermally (A4, A7) and the cyclically grown oxide microstructure was evident in the areas where the oxide remained adherent. The net mass gain curves (when measured) are given on Fig. 6. The shape of the curves is characteristic of the competition between spalling and oxidation [2,10–12]. Careful analysis of experimental mass recorded during TGA tests was performed as described in the section devoted to spalling evaluation. Fig. 7 is an example of the results obtained. S.E.M. observations showed that spalling occurred at the metal-oxide interface. For cyclic and isothermal oxidations, interfacial cavities were observed for both surface orientations. These kinds of voids have been often reported [2,13–19]. Laue diffraction technique analysis of the single crystal and S.E.M. observations at different tilts angles have shown that facets are formed along specific crystallographic planes. Measuring the apparent width of crystallographical surface at different tilt angles allowed orientation to be identified because the orientations of the sample surface and of a particular direction were known. This method showed that most of the void facets corresponded to the {1 1 0} planes in

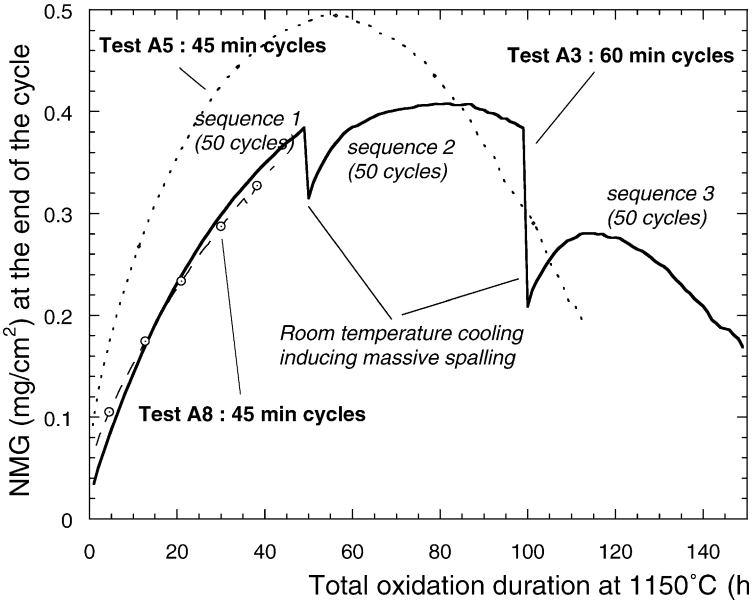

Fig. 6. Cyclic oxidation. Net mass gain curves obtained at 1150 °C.

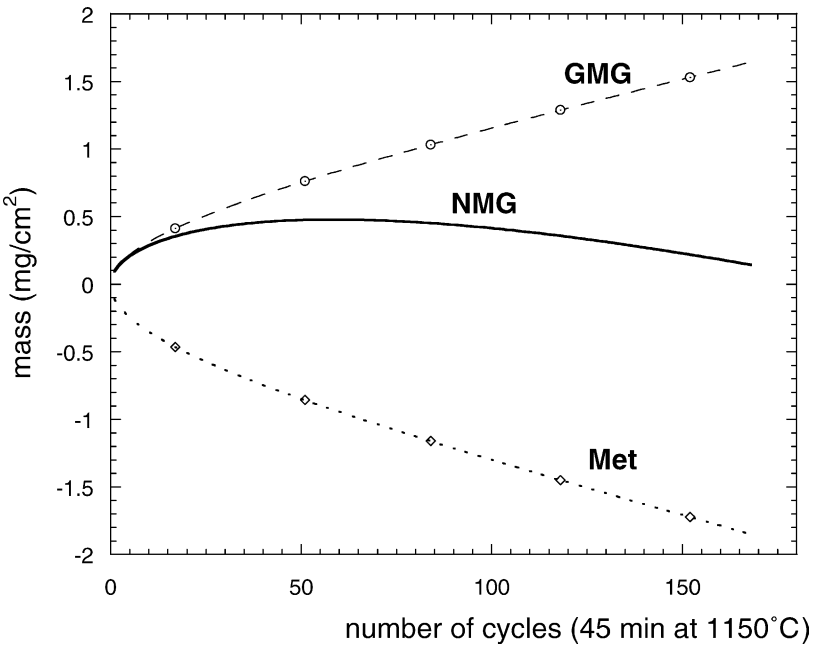

Fig. 7. Cyclic oxidation. Experimental (NMG) and calculated (GMG, Met) curves obtained using thermogravimetry in cyclic conditions for test A5.

β-NiAl. However, some {1 1 2} planes were also evidenced (Fig. 8). Spiral steps (Fig. 3) on the β-NiAl cavities have been observed on both orientations, for isothermal and for cyclic oxidation, as in [2,14]. Oxide above the voids was never observed to be thinner than the oxide in contact with the metal. As a result, it is suggested that the vapor transportation of aluminium from the void surface to the oxide could explain both the spiral steps and the constant oxide thickness [19].

S.E.M. observation of cyclic oxidation specimens revealed that oxide spalled locally (10–20 μm diameter flakes), leaving a bare surface. Interfacial cavities were present on the bare metal. These interfacial cavities had a certain roughness which will be again covered by a new

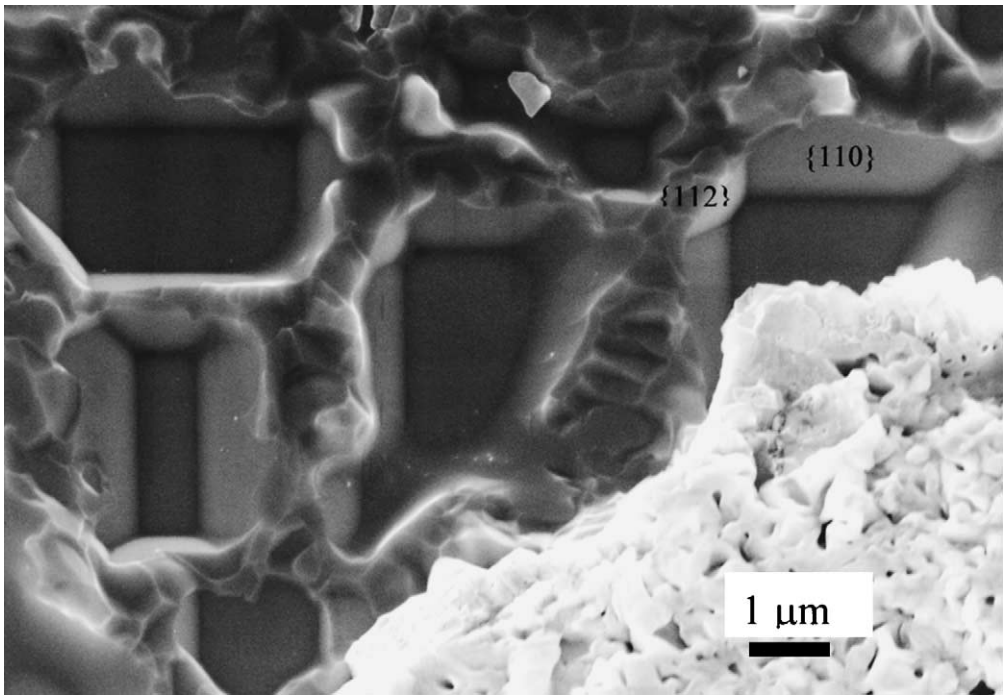

Fig. 8. Cyclic oxidation (Test A17, 20 cycles of 45 min at 1150 °C in flowing O_2). S.E.M.–S.E. observation of the (1 1 0) surface.

oxide (Fig. 1). S.E.M. observations were performed with several acceleration voltages (5–30 kV) in order to show oxide flakes with different thicknesses. These observations are useful but these results cannot be used to quantify spalling during inter-cycle cooling as massive spalling occurred when the sample was cooled to room temperature to be analyzed and observed, as shown by experiment A3 (Fig. 6).

Even for short isothermal oxidation tests, and small oxide thickness (450–500 nm) massive spalling was observed. For test A8, at the end of cycle 48, the sample was cooled to 15 °C instead of 150 °C. During this cooling 1.1% in mass of the oxide spalled, which is one order of magnitude above the average value at the previous cycles. Test A3 had also two excursions to 15 °C instead of 150 °C but for longer duration (10 h instead of 15 min). During these excursions, 9% and then 16% in mass of the oxide was spalled. These particular sequences show that the value of the cold temperature has to be taken into account as well as the amplitude of the thermal cycle (ΔT = 1150–150 °C). In [20], Evans reviewed the effect of ΔT cooling on spallation. This point has also been studied by Deadmore and Lowell [21,22]. Simpson and Evans [23] have proposed that the quantity of spalled oxide s on a chromia forming austenitic steel was related to the mass gain before spalling w and to the temperature drop ΔT by:

$$s = Aw + Bw^2\Delta T^2 + Cw^3\Delta T^4 + Dw^4\Delta T^6 \quad (5)$$

The weight of spalled oxide is a function of the growth weight gain. This model, applied in [24] gives good results. In our case, a small increase of ΔT from 1000 to 1100 K leads to a dramatic increase of s. The driving force for additional spallation is both the thermal expansion stress deriving from ΔT and the increasing humidity at lower T_{min}. This is contrasted with the view of more spallation simply based on higher T_{max}. Intentional exposure to moisture was found to increase the spalling rate [25–28]. If 100 °C appears to be a critical level for the cold temperature of the cycle, it would be interesting to focus on the influence of water on spalling, even for small quantities of H_2O. More experimental results are needed with cautious in situ spalling measurement to better understand this particular point.

Spalling was analyzed as proposed in [7] and recalled at the beginning of this article. The results for spalling at each cycle are plotted for the three tests as shown in Figs. 9 and 10, which give the proportion P_n of oxide spalled at cycle number n. For test A8, P_n values lay in the range 0.09–0.25% and slightly increased with the number of cycles. As already mentioned, the cold temperature of the cycle was lowered to 15 °C for cycle 48 and this modification resulted in a massive spalling of 1.1%. It is interesting to note that spalling recovered to the previous level afterwards. During the four first cycles, mass gain due to oxidation during cooling and heating was larger than the mass loss due to spalling so that the values on the curve (Fig. 9) are negative. Tests A3 and A5 (Fig. 10) showed similar results.

In Fig. 10, for tests A3 and A5 which were longer than test A8, spalling increased quite linearly during the first 110 cycles and then seemed to stabilize at about 0.9%. Tests A5 and A3 were made using the same crystallographic orientation of the oxidizing surface and differed only with regards to the dwell time (respectively, 45 and 60 min). If, as shown in Fig. 6, the net mass gain curves obtained are plotted as a function of the number of cycles instead of the total oxidation duration, then it can be seen that the curves are

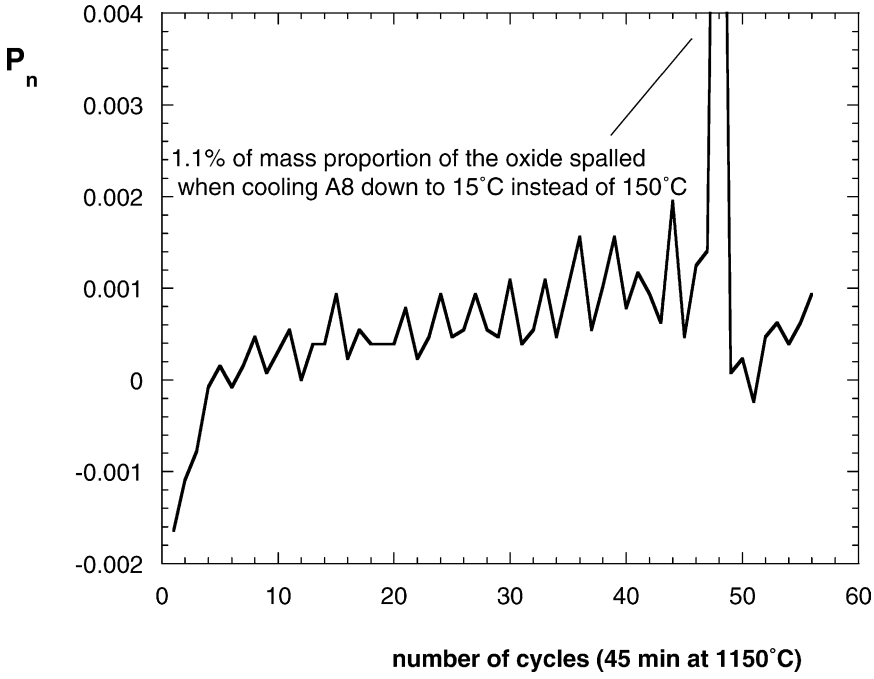

Fig. 9. Cyclic oxidation. Spalling data for test A8 (P_n is the mass proportion of the oxide spalled at each cycle).

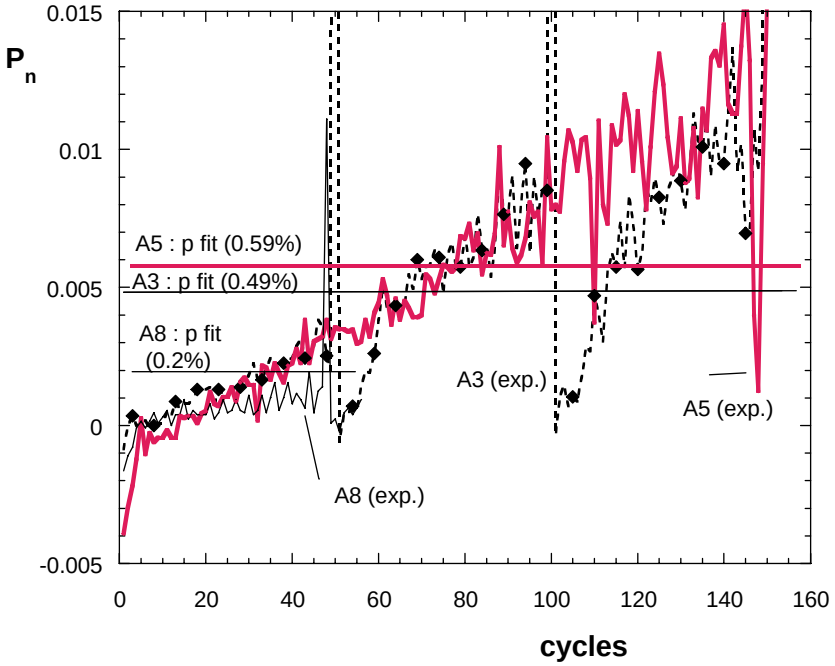

Fig. 10. Cyclic oxidation. Spalling of NiAl in flowing O_2 (45 min cycles for A8 and A5 and 60 min cycles for A3). P_n is the mass proportion of the oxide spalled at each cycle. Experimental values of P_n are to compare with p used in the p–k_p model.

quite close. The time at high temperature is an important parameter to be taken into account, especially when longer cycle times are studied, such as for land-based gas turbine engine for power generation, but the difference between 45 and 60 min dwells is quite small and the number of cooling sequences prevails.

Finally, pseudo-k_p can be calculated from the experimental data obtained during cyclic oxidation tests, using the small net mass gain curve obtained at each dwell time during cyclic oxidation [7]. The results are given in Table 4. The values obtained are rather constant, taking into account the low precision due to very small mass gains from which these values were calculated. These results are consistent with the expected k_p evolution with time at 1150 °C, due to constant oxide microstructure and k_p when the steady state between oxide formation and spalling is reached (as explained in [4]).

When these pseudo-k_p values are compared with those obtained at the same temperature during tests A4 and A7, it is apparent that isothermal testing leads to k_p values similar to those given in Table 4, except for A10 and A15 which were oxidized for short times and then experienced faster oxidation kinetics due to the formation of transient alumina.

3.3. Orientation effect

The crystallographic surface orientation has an influence on oxidation kinetics (Fig. 2). During isothermal tests, both at 1050 and 1150 °C, oxidation kinetics of the (1 0 0) oriented surface were slightly faster than on the (1 1 0) oriented surface. Surface orientation was the only difference between cyclic oxidation tests A5 and A8. Spalling is also slightly larger for the (1 0 0) surface. As oxidation kinetics were more important with this surface orientation, the hypothesis of higher spalling P_n with a larger oxide thickness appears to be the simplest hypothesis to explain the experimental results. During cyclic oxidation tests NMG curves of (1 0 0) oriented surface were always above NMG curves for the (1 1 0) oriented surface. However, kinetics differences between the (1 0 0) and (1 1 0) surfaces were small and further investigations are necessary before any definitive conclusion on this topic can be drawn. Few studies are available on the effect of crystallographic orientation of the oxidizing surface on oxidation kinetics on alumina forming alloys. In [29] Doychak et al. focused on the transient oxidation of β-NiAl in air at 800 °C and 1100 °C. At 800 °C,

Table 4
Cyclic oxidation tests at 1150 °C, k_p ($mg^2\,cm^{-4}\,s^{-1}$) calculated on the small curve obtained at each dwell time

Sample	Cycle 2	Cycle 20	Cycle 48	Cycle 90	Cycle 150
A3 (1 0 0)	3.8×10^{-7}	1.5×10^{-6}	3.8×10^{-7}		
A5 (1 0 0)	5.2×10^{-7}	2.9×10^{-7}	1.3×10^{-7}	2.9×10^{-7}	4.1×10^{-7}
A8 (1 1 0)	1.8×10^{-7}	3.5×10^{-7}	2.0×10^{-7}		

These values overestimate local oxidation kinetics.

Table 5
Cyclic oxidation tests (values obtained after the automatic fitting procedure)

Sample	Orientation	Temperature (°C)	p (%)	k_p (mg^2 cm^{-4} s^{-1})
A3	(1 0 0)	1150	0.49	1.4×10^{-6}
A5	(1 0 0)	1150	0.59	3.5×10^{-6}
A8	(1 1 0)	1150	0.20	1.3×10^{-6}
A12	(1 0 0)	1050	0.05	3.0×10^{-6}

for (1 0 0) oriented surfaces $k_p = 1.1 \times 10^{-7}$ mg^2 cm^{-4} s^{-1}, for (1 1 0) oriented surfaces $k_p = 0.8 \times 10^{-7}$ mg^2 cm^{-4} s^{-1}. At 1100 °C, they indicate that oxide scale was 'thicker for equal oxidation time' on (1 1 0) oriented surfaces than on (1 0 0) oriented surfaces. The chemical composition of the β-NiAl single crystal used and surface preparation (600 grit surface) differed from those used in our study. In [30], at 1100 °C, crystal orientation of a single-crystalline β-NiAl in oxygen has practically no influence on the oxidation rate. However, in that study, (1 1 0) oriented surface NMG curves are above (1 0 0) oriented surface NMG curves.

3.4. Modelling cyclic oxidation tests

The model detailed in [4] was applied to cyclic oxidation tests A3, A5, A8, A12. Assuming that the parabolic constant k_p and the proportion of surface spalled at each cycle p do not vary with the number of cycles, the values were obtained after the automatic fitting procedure and are given in Table 5.

The simulation curves calculated from these values and the experimental data are plotted in Fig. 11, which indicates that the experimental data are not very well fitted by the model. The first reason for that discrepancy is that P_n, the experimental spalling ratio is not constant as shown by the continuous thermogravimetry analysis (Fig. 10). As detailed earlier, P_n increased with the increasing number of cycles. In the proposed simplified model, spalling ratio p was assumed to be constant. As a result, the simulation overestimated spalling at the beginning of the test and underestimated spalling at the end of the test. The second parameter used in the model is k_p. The values obtained from the model (Table 5) given above are approximately twice the values measured during isothermal oxidation tests at the same temperature, using the same material and with the same surface orientation. In fact, this point can be easily related to the previous one. As the simplified model leads to an overestimation of spalling at the beginning of the curve, an overestimation of k_p is necessary to fit experimental data. Furthermore, the k_p values identified come from an average between those of θ-alumina and of α-alumina, because cyclic oxidation may emphasize transient alumina formation.

To analyze the spalling extent as a function of the average oxide thickness, the mass of oxide spalled per cycle (S^n_{OX}) versus the mass of adherent oxide (A^n_{OX}) was plotted on Fig. 12. Fig. 12 clearly shows an asymptotic value for A^n_{OX}. This asymptotic behavior is consistent with a stationary state reached when the oxide spalled at each cycle compensates for the oxide grown during each cycle. This balance is evidenced with A^n_{OX} which reaches a constant value, i.e. the average oxide thickness is constant (but the thickness is not uniform over the surface). This value of the average oxide thickness is about 2.5 μm for our experiment. At this point, one could wonder if this constant average oxide thickness is related to the concept of critical oxide thickness,

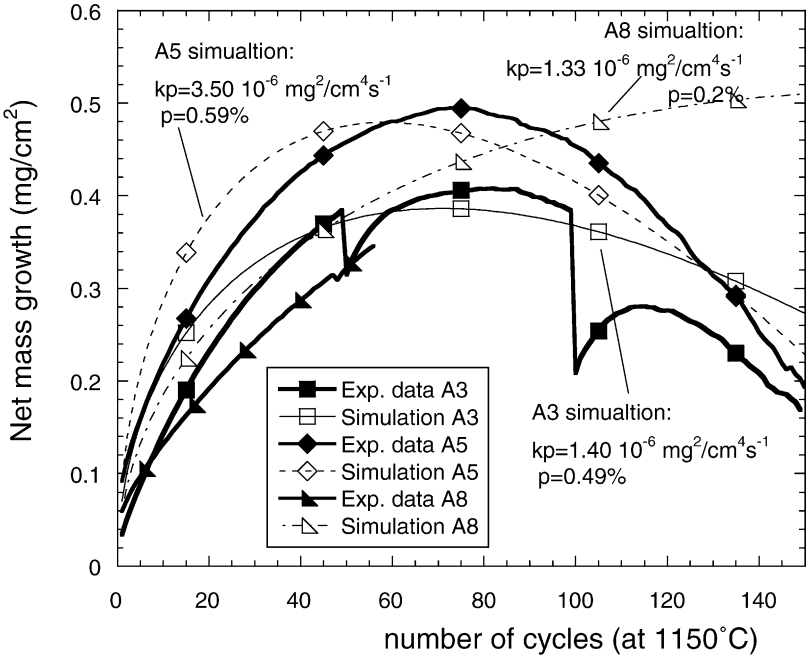

Fig. 11. Cyclic oxidation tests. p–k_p modelling compared to experimental data.

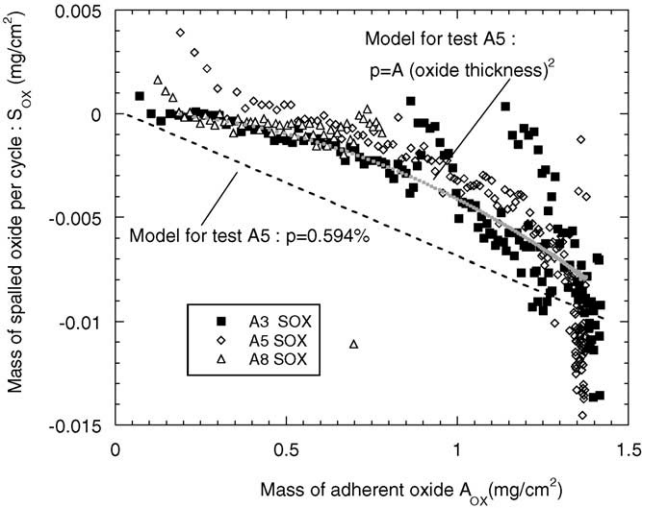

Fig. 12. Cyclic oxidation of NiAl in flowing O_2. Spalling data for tests A3, A5 and A8 (mass of spalled oxide at each cycle as a function of the mass of the adherent oxide).

as in [31], where Meier and coworkers reported a value of 7.6 μm as a critical TGO thickness on a Ni(Pt)Al bond coat, in a study concerning thermal barrier coating life prediction, at the same temperature. Perhaps critical oxide thickness is more typical of adherent scale formed on Pt,Y-doped alloys, but our experimental data do not support a model based only on a critical oxide thickness. Actually, Figs. 10 and 12 show that spalling probability cannot be taken as constant, but also that a critical oxide thickness used as a spalling criterion as in [32,33] does not fit the experimental data obtained. Also, Fig. 10 shows that spalling occurs since the first cycles. As a result, value of the spalling probability as a power law of the oxide thickness would be more suitable, as allowed in COSP model [11,12]. However, oxidation has proceeded beyond the transient stage when tests are performed for enough cycles, the model (constant values for p and k_p) fits the mass gain curves very accurately [4]. That means that after the net mass gain curve reaches its maximum and starts to decrease, the linearity of the NMG curve indicates that the mass of oxide formed equals the mass of oxide spalled during each cycle. As a result, the distribution of oxide thickness remains the same, which may imply a constant value of the spalling ratio.

Fig. 12 also indicates that spalling increases faster with the average oxide thickness than a linear function. Thus, these points explain that a model, that assumes a constant value of p and a constant value of k_p, cannot accurately fit the present experimental curves. An increase in spall fraction with oxide thickness has previously been reported for NiAl by Smialek [2]. In Smialek's work, spall fraction, measured by S.E.M. at room temperature varies as (oxide thickness)$^{1.5}$ for 1 h cycle tests and as (oxide thickness)^2 for isothermal tests. The matter was that the value of the spalling measured appears to be three times the value obtained by fitting the NMG curves. This was explained by the fact that spalling measure is dependent on the duration of sample exposure to laboratory air (moisture effect) before S.E.M. observations. For 1 h cyclic tests carried out at 1100 °C on Ni-42Al, the value of spalling (k_s = 0.12–0.16%) obtained by Smialek when he fits his model can be compared to the p values obtained in this study and detailed above (p = 0.2–0.5% at 1150 °C). The difference between both results could be due to the fact that spalling probability is highly dependant on chemical composition of the sample and especially on sulfur content.

To obtain a better fit of these relatively short cyclic oxidation data, which emphasize the stage when the average thickness of the scale is increasing, a numerical simulation is necessary. Numerical simulation allows the definition of p as a function of the local oxide thickness. This function may be deduced from the experimental data given in Fig. 10. Such a procedure using cyclic thermogravimetry and Monte Carlo numerical modelling is presented in [34]. Spall fraction p as a function of (oxide thickness)^2 gives better result than those obtained with p independent of oxide thickness (Fig. 12).

The last point to discuss is the effect of the dwell time. As explained above, in the comparison of tests A3 and A5, a decrease in dwell duration of 25% resulted in no significant modification of the experimental mass gain curves. In [2], Smialek studied the effect of cycle duration (1, 5, 20, and 50 h cycles) on Ni-42Al at oxidation kinetics. For an equal amount of test time spent at 1100 °C, the 20 h cycle test was more severe than the 50 h cycle test and than the 1 h cycle test. In [35], in which, 1, 10 and 100 h cycle tests have been carried out on Ni-51Al at 1200 °C, the influence of this parameter is difficult to model as only a slight increase in the linear spallation rates was shown when the cyclic time was decreased from 100 to 1 h. In the model applied here (assuming constant p and k_p), the final linear slope of the net mass gain (mass versus cycles) curve must increase as the square root of the dwell time. But, if the net mass gain curve is plotted as a function of the total time spent at high temperature instead of as a function of the number of cycles, then, the model predicts that the net mass gain curve must decrease as the square root of the dwell time. In our case, the fit of the simple (p, k_p) model gives comparable values of p and k_p for both tests because the dwell time difference is too small.

4. Conclusion

Oxidations tests have been performed under different experimental conditions on β-NiAl single crystal. Oxide scale microstructures obtained were in agreement with data available in the literature. For all the isothermal and cyclic tests carried out in this study, (1 0 0) oriented surfaces appeared to oxidize slightly faster than (1 1 0) oriented surfaces. The extent of spalling was shown to depend strongly on the temperature of the low-temperature dwell. A specific

methodology was applied to cyclic tests in order to evaluate oxidation kinetics at each cycle and oxidation spalling during each cooling. This methodology showed that spalling probability is increasing with the number of cycles in the first stage of cyclic oxidation, when the average oxide scale thickness was increased with the number of cycles. Longer tests are necessary to study this evolution during the 'steady-state' but no critical oxide thickness was found. Indeed our results are best modelled by a transient stage when the spalling fraction increases with the square of the increasing oxide scale thickness, followed by stationary stage when the average oxide scale thickness is constant as well as the spalling fraction and the oxidation kinetics.

Acknowledgements

The authors would like to thank M.P. Bacos and P. Josso from O.N.E.R.A. (Chatillon, France) for providing the NiAl single crystal. C. Levade, from INSA Toulouse and D. Caillard from CEMES are sincerely acknowledged for providing respectively Laue diffraction and spark machining facilities. This study was partly funded by the French Research Ministry grant "ACI 2000 Surfaces and Interfaces" (AdhéronS!).

References

[1] M. Brady, B. Pint, P. Tortorelli, I. Wright, R. Hanrahan, High temperature oxidation and corrosion of intermetallics, in: Materials Science and Technology: A Comprehensive Treatment, vol. 19B, Corrosion and Environmental Degradation of Materials, Wiley–VCH, Weinheim, Germany, 2000, p. 229.
[2] J.L. Smialek, Metall. Mater. Trans. 9A (1978) 309.
[3] J. Doychak, C.A. Barrett, J.L. Smialek, in: V. Srinivasan, K. Vedula (Eds.), Corrosion and Particule Erosion at High Temperatures, The Minerals Metals and Materials Society, Warrendale, 1989, p. 487.
[4] D. Poquillon, D. Monceau, Oxid. Met. 59 (3/4) (2003) 409.
[5] D. Monceau, K. Bouhanek, R. Peraldi, A. Malie, B. Pieraggi, J. Mater. Res. 15 (2000) 665.
[6] D. Monceau, B. Pieraggi, Oxid. Met. 50 (1998) 477.
[7] D. Monceau, D. Poquillon, Oxid. Met. 61 (2004) 143.
[8] M.W. Brumm, H.J. Grabke, Corros. Sci. 33 (1992) 1677.
[9] A. Andoh, S. Taniguchi, T. Shibata, in: Proceedings of the High Temperature Corrosion and Protection of Materials International Symposium (HTPCM 5), Les Embiez, France, Trans Tech Publications, vols. 369–372, 2001, p. 303.
[10] C.E. Lowell, J.L. Smialek, C.A. Barrett, in: Proceedings of the International Conference on High Temperature Corrosion, San Diego, CA, 2–6 March 1981, National Association of Corrosion Engineers, 1983, p. 219.
[11] C.E. Lowell, C.A. Barrett, R.W. Palmer, J.V. Auping, H.B. Probst, Oxid. Met. 36 (1991) 81.
[12] J.S. Smialek, J.V. Auping, Oxid. Met. 57 (2002) 559.
[13] D. Oquab, D. Monceau, Scripta Metall. Mater. 44 (2001) 2741.
[14] H. Hindam, W. Smeltzer, J. Electrochem. Soc. 127 (1980) 1630.
[15] J.A. Haynes, M.J. Lance, B.A. Pint, I.G. Wright, Surf. Coat Technol. 146 (2001) 140.
[16] J.K. Doychak, in: Proceedings of the International Congress on Metallic Corrosion, vol. 1, Toronto, 1984, p. 35.
[17] J. Doychak, M. Ruhle, Oxid. Met. 31 (1989) 431.
[18] D. Oquab, D. Monceau, in: Proceedings of the High Temperature Corrosion and Protection of Materials International Symposium (HTPCM 5), Les Embiez, France, Trans Tech Publications, vols. 369–372, 2001, p. 499.
[19] J. Tien, F. Pettit, Metall. Trans. 3 (1972) 1587.
[20] H.E. Evans, Int. Mater. Rev. 40 (1995) 1.
[21] D. Deadmore, C. Lowell, Oxid. Met. 11 (1977) 91.
[22] C.E. Lowell, D.L. Deadmore, Oxid. Met. 14 (1980) 325.
[23] P. Simpson, H. Evans, in: Nuclear Fuel Performance, British Nuclear Energy Society, London, 1985.
[24] J. Jedlinski, M.J. Bennet, H.E. Evans, Mater. High Temp. 21 (1994) 169.
[25] J.L. Smialek, Metall. Mater. Trans. 22A (1991) 739.
[26] M.A. Smith, W.E. Frazier, B.A. Pregger, Mater. Sci. Eng. A203 (1995) 388.
[27] R. Janakiraman, G.H. Meier, F. Pettit, in: M. Schutze, W.J. Quadakkers (Eds.), Cyclic Oxidation of High Temperature Materials, vol. 27, European Federation of Corrosion, Frankfurt/Main, 1999, p. 38.
[28] J.L. Smialek, G.N. Morscher, Mater. Sci. Eng. A332 (2002) 11.
[29] J.K. Doychak, J.L. Smialek, T.E. Mitchell, Metall. Mater. Trans. A20 (1989) 499.
[30] St. Mrowec, A. Gil, J. Jedlinski, Werkst. Korros. 38 (1987) 563.
[31] S.M. Meier, D.M. Nissley, K.D. Sheffler, T.A. Cruse, J. Eng. Gas Turb. Power 114 (1992) 258.
[32] H.E. Evans, R.C. Lobb, Corros. Sci. 24 (1984) 209.
[33] H.E. Evans, Mater. High Temp. 12 (1994) 219.
[34] D. Poquillon, D. Oquab, D. Monceau, in: Proceedings of the High Temperature Corrosion and Protection of Materials International Symposium (HTPCM 6), Les Embiez, France, Trans Tech Publications, Materials Sciences Forum, 2002.
[35] B.A. Pint, P. Tortorelli, I.G. Wright, Oxid. Met. 58 (2000) 73.